Local Chirality of Optical Resonances in Ultrasmall Resonators

Brandon Redding, Li Ge, Qinghai Song, Jan Wiersig, Glenn S. Solomon, and Hui Cao

Phys. Rev. Lett. **108**, 253902 — Published 19 June 2012

DOI: 10.1103/PhysRevLett.108.253902

Local chirality of optical resonances in ultrasmall resonators

Brandon Redding[1], Li Ge[2], Qinghai Song[3], Jan Wiersig[4], Glenn S. Solomon[5], Hui Cao[1]

[1] *Department of Applied Physics, Yale University, New Haven, CT 06520, USA*

[2] *Department of Electrical Engineering, Princeton University, Princeton, New Jersey 08544, USA*

[3] *National Key Laboratory of Tunable Laser Technology, Institute of Opto-Electronics, Harbin Institute of Technology, Harbin, 150080, China*

[4] *Institut für Theoretische Physik, Universität Magdeburg, Postfach 4120, D-39016 Magdeburg, Germany*

[5] *Joint Quantum Institute, NIST and University of Maryland, Gaithersburg, Maryland 20899, USA*

(Dated: April 24, 2012)

Abstract

In wavelength-scale cavities with chiral-symmetric geometry, wave optical effects can introduce local chirality; that is, a spatial separation of the clockwise (CW) and counter-clockwise (CCW) propagating resonant modes. We show that this local chirality results in unidirectional lasing emission in the far-field. In the presence of a waveguide, the local chirality also allows for directional evanescent coupling of the lasing modes, and the output direction can be varied by selecting the coupling position along the cavity boundary. Our results demonstrate that the local chirality of optical resonances can be utilized to control the output directionality and enhance the collection efficiency of emission from ultrasmall resonators.

Chirality has important implications in many areas of physics including optics. Typically, chirality is introduced via structural geometry with distinct left- and right-handed forms. In this Letter, we will demonstrate in two-dimensional (2D) optical resonators that, even if the structure has chiral symmetry [$r(-\theta) = r(\theta)$, where $r(\theta)$ describes the cavity boundary in polar coordinates], the local balance between the amplitudes of clockwise (CW) and counterclockwise (CCW) propagating waves may still be broken. As an example, a dielectric microdisk can confine light by total internal reflection (TIR) from the disk boundary enabling high quality factors and low lasing thresholds [1]. If the microdisk is perfectly circular, the rotational symmetry of the cavity shape leads to isotropic output, which hinders light collection. One approach to break the rotational symmetry is positioning a waveguide (or fiber) sufficiently close to the cavity to allow the emission to couple to the waveguide evanescently [2–4]. The balance between the amplitudes of the CW and CCW propagating beams in the cavity is preserved and the energy coupled out is split evenly into the two waveguide directions. Unidirectional coupling to a waveguide can be achieved by breaking the chiral symmetry of the cavity shape [$r(-\theta) \neq r(\theta)$], e.g. using a spiral-shaped cavity [5–8]; however, this approach results in a significant reduction in the quality factor ($Q = \omega/\Delta\omega$, where ω is the resonance frequency and $\Delta\omega$ is the linewidth).

An approach to achieve non-isotropic emission without introducing a waveguide is to deform the cavity from a circular shape [9–21]. In most cases studied so far, the deformation does not break the chiral symmetry of the cavity shape. Nonetheless, directional emission is possible when the rotational symmetry is removed. If the disk radius R is much larger than the optical wavelength λ (in vacuum), the output directionality is determined by the intracavity ray dynamics, which can be manipulated via deliberate deformation of the cavity shape [22] to produce emission in a single direction [17]. Recently, wavelength-scale deformed cavities have been fabricated in efforts to reduce the cavity mode volume [23]. As kR ($k = 2\pi/\lambda$) approaches one, the classical ray model breaks down, and wave optical phenomena become significant. High-Q modes may be formed by partial barriers in the phase space [24], and their emission (to free space) is not as directional as from larger cavities. The only method that has been shown to generate unidirectional output from such small cavities is accidental coupling of an isotropic high-Q mode (HQM) to an anisotropic low-Q mode (LQM) [23]. In this Letter, we will show that when we move further into the wave regime by making the cavity even smaller, the HQMs become directional again, in the absence of

mode coupling. Such behavior is attributed to the breaking of the local balance between CW and CCW wave intensities, i.e. $I_{CW}(\theta) \neq I_{CCW}(\theta)$ at the cavity boundary. This local chirality, defined as $W(\theta) \equiv [I_{CW}(\theta) - I_{CCW}(\theta)]/[I_{CW}(\theta) + I_{CCW}(\theta)]$, is introduced by wave optical effects such as "Goos-Hänchen" shift (GHS) and "Fresnel Filtering" (FF) [25–30]. It also enables unidirectional coupling to a waveguide, and the output direction can be varied by selecting the coupling point on the cavity boundary. Experimentally, we realized lasing at kR as small as 3, and observed unidirectional emission from the lasing modes. In addition, we demonstrated selective coupling of the CW or CCW waves in a lasing mode to a waveguide placed tangential to the disk boundary. The combination of relatively high-Q factor, small mode volume, and in-plane directional emission or directional waveguide coupling are appealing not only to the fundamental studies of cavity quantum electrodynamics, but also to the developments of nanophotonic devices such as ultrasmall light sources, optical switches and sensors.

Though our results are relevant for a variety of deformed cavities deep in the wave optics regime, we focused on the limaçon cavity whose boundary is described by $r(\theta) = R(1+\epsilon\cos\theta)$ and preserves the chiral symmetry $r(-\theta) = r(\theta)$. The refractive index of the cavity is set at $n = 3.23$, to be consistent with the effective index of the GaAs disks in our experiment. In the semiclassical regime ($kR \gg 1$), the HQMs in the limaçon cavity have unidirectional emission, dictated by the chaotic ray dynamics in an open cavity [17]. The universal directionality diminishes at smaller kR when the ray model fails, and only accidental coupling to a directional LQM makes the output from a HQM unidirectional at $5 < kR < 25$ [23]. Here we investigated the behavior of the resonant modes deep into the wave regime $2 < kR < 5$ using the finite element method (COMSOL Multiphysics 3.5a) and the scattering matrix method [31]. Only transverse-electric (TE) polarized modes are considered, because experimentally the lasing modes are usually TE polarized due to the stronger vertical confinement (index guiding) and larger amplification by the InAs quantum dots (QDs) in the GaAs disks. In Fig. 1, the circles represent the highest Q modes (HQMs) within the frequency range of interest in a cavity of $\epsilon = 0.41$, and the squares represent the lower Q modes (LQMs). The HQMs resemble whispering gallery modes of radial number equal to one, whereas the LQMs have radial number equal to two [32]. The Q values for both modes show the tendency of increasing with kR. For $3.6 < kR < 4.1$, the HQMs nearly coincide with the LQMs in frequency, and their coupling results in a dip in the Q of the HQM series [32]. Away from

the coupling regime, the HQMs have better output directionality than the LQMs, as characterized by $U \equiv \int I(\theta)\cos\theta d\theta / \int I(\theta) d\theta$, where $I(\theta)$ represents the angular distribution of the far-field intensity. [$U = 0$ corresponds to isotropic or bidirectional emission, whereas positive (negative) U corresponds to emission primarily towards $\theta = 0°$ (180°). The factor $\cos\theta$ in the integrand also allows the value of U to reflect to some degree how "peaked" the unidirectional emission is.] The behavior shown in Fig. 1(b) is the opposite of what was observed previously in the regime of larger kR (e.g., $5 < kR < 25$), where the HQMs have lower U than the LQMs except when they are coupled [23]. Hence, deeper into the wave regime ($2 < kR < 5$), the HQMs regain directionality when they are *decoupled* from the LQMs. In fact, coupling to the LQMs is detrimental, because the LQMs are no longer directional. Such behavior is desirable as it means that the lasing modes, which usually correspond to the HQMs, can have directional emission without the Q reduction (and increased lasing threshold) associated with coupling to the LQMs.

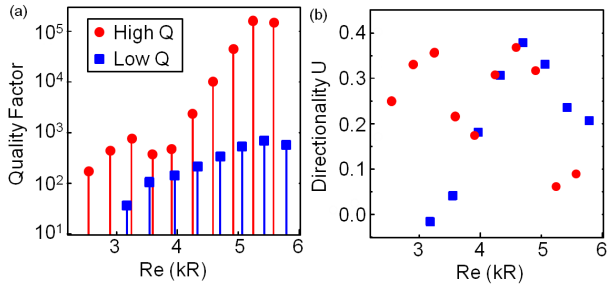

FIG. 1. (color online). Calculated Q factor (a) and emission directionality U (b) of the highest Q modes (circles) and lower Q modes (squares) as a function of kR in a limaçon cavity of $\epsilon = 0.41$ and $n = 3.23$. The highest Q modes have better emission directionality than the lower Q modes deep in the wave regime $2 < kR < 5$, except when the two are coupled near $kR = 4$.

To understand the behavior of the HQMs, we extracted the constituent CW and CCW waves by decomposing the field distribution. For a TE mode, it is easier to use the magnetic field component which is perpendicular to the disk plane (parallel to the z axis). Inside the cavity $H_z(r,\theta) = \sum_m a_m J_m(kr) e^{im\theta}$, and outside the cavity $H_z(r,\theta) = \sum_m b_m H_m^{(1)}(kr) e^{im\theta}$, where J_m is the mth-order Bessel function, and $H_m^{(1)}$ is the first-kind Hankel function that represents an outgoing wave. $m > 0$ corresponds to CW propagating wave and $m < 0$ to CCW; hence, the CW field amplitude can be obtained by summing over all positive m's, and the CCW over all negative m's. As an example, Fig. 2(a) plots the intracavity CW wave

intensity for a HQM of $kR = 3.2$. It clearly shows that the CW wave has enhanced amplitude at three locations on the cavity boundary, which are close to but not coincident with the bouncing points of a "triangle" orbit predicted by ray optics (black dashed line). A similar phenomenon is seen for the CCW wave in Fig. 2(b), although its intensity is enhanced at different locations. The spatial separation of the CW and CCW intensity maxima results in the local chirality $W(\theta)$, which is plotted as a function of the polar angle θ along the cavity boundary in Fig. 2(e).

To identify the physical origin of the local chirality, we calculated the Husimi projection onto the classical surface of section (SOS), which provides the ray content of this mode in terms of the density of rays and their angles of incidence and reflection at the cavity boundary. The incident and emergent Husimis show enhanced density at three locations on the boundary [32], allowing us to extract the center positions of the incident and reflected beams at the cavity boundary and reconstruct the orbits shown as solid lines in Fig. 2(a,b). The position of the bounces from the Husimi projection agrees well with the real-space wave pattern, which is surprising at $kR \sim 3$ since the Husimi distributions are derived with the assumption that $kR \gg 1$ [33]. Nevertheless, the Husimi distributions clearly show the presence of two wave effects in our system: GHS and FF [25–30]. Both effects result from the angular spread of an optical beam. The GHS is a lateral displacement of the center of the reflected beam from that of the incident beam along the cavity boundary, and the FF causes the reflection angle of the beam center to be larger than the incident angle. These effects break the spatial degeneracy of the CW and CCW waves, introducing local chirality. For the CW beam [Fig. 2(a)], the incident angle at bounce 1 is smaller than the incident angle at bounce 3, light leakage from bounce 1 exceeds that from bounce 3. This is confirmed in Fig. 2(c) which highlights the CW wave intensity outside the cavity and reveals that the output from bounce 1 is stronger than that from bounce 3. Similarly, the escape of the CCW beam from bounce 3 is larger than from bounce 1. In both cases, the enhanced outputs are in the $\theta \sim 0^\circ$ direction, combining to provide unidirectional emission.

We have investigated HQMs in limaçon cavities of different ϵ [32], and observed local chirality at small kR producing directional output. This can be understood from our previous study on partial barriers in phase space [24]: as kR decreases, the underlying orbits for the HQMs have decreasing number of bounces and the angles of incidence approach the critical angle for total internal reflection. In the regime of $2 < kR < 5$, the HQMs correspond to

triangle orbits close to the critical line in the SOS, thus the wave effects (FF and GHS) are strong enough to create local chirality. However, the FF and GHS cannot be estimated quantitatively in our case, because they are originally applied to optical rays at $kR \gg 1$ and the "extended" ray dynamics that include the first-order wave corrections at lower kR [30] does not work at such small values of kR. Nevertheless, optical beams do propagate in our cavities and experience stronger FF and GHS than in the larger cavities, leading to the local chirality.

To confirm the relation of local chirality and emission directionality, we investigated a HQM at $kR = 5.2$ which does not possess local chirality. Decomposition of this mode into CW and CCW waves reveals that it corresponds to the diamond orbit with four bounces from the cavity boundary [Fig. 2(d)]. However, the spatial separation of CW and CCW beams is negligible. As a result, the local chirality W is near zero for all θ, as shown in Fig. 2(e). The far-field emission intensity distribution $I(\theta)$ is non-directional [Fig. 2(f)], in contrast to the mode of $kR = 3.2$. This illustrates the essential role played by the local chirality in producing unidirectional emission at small kR.

Next, we experimentally confirm the unidirectional emission from the lasing modes in ultrasmall limaçon cavities. Our sample fabrication procedure and experimental lasing characterization setup are similar to those reported in ref. [18]. Briefly, GaAs disks of limaçon shape were fabricated by electron-beam lithography, reactive ion etching and selective wet chemical etching. The disks are 265 nm thick and supported by $Al_{0.7}Ga_{0.3}As$ pedestals in the center. InAs QDs embedded in the GaAs disk were optically excited to provide gain for lasing. Figure 3 presents the lasing result for a limaçon cavity of $R = 460$ nm and $\epsilon = 0.41$ (the same shape as in Figs. 1 and 2). A scanning electron microscope (SEM) image of this disk (top view) is shown in the inset of Fig. 3(a). The emission peak at $\lambda = 875$ nm in the spectra of Fig. 3(a) corresponds to the cavity resonance at $kR = 3.2$ in Figs. 1 and 2. Its intensity displays a threshold behavior as the pump power increases [Fig. 3(b)]. The measured far-field pattern [inset of Fig. 3(b)] reveals that the emission is predominantly in the $\theta = 0^\circ$ direction, in good agreement with the numerical simulation. In addition, we observed another mode at $kR = 2.98$ ($\lambda = 970$ nm) which also exhibited unidirectional emission towards $\theta = 0^\circ$. We repeated the lasing experiments with different limaçcon cavities, and observed similar phenomena deep in the wave regime.

The local chirality also offers an opportunity to selectively couple light that propagates

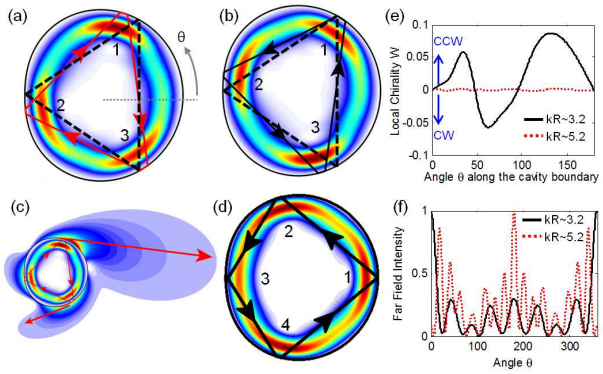

FIG. 2. (color online). (a,b): Calculated spatial intensity distribution of the CW (a) and CCW (b) waves that constitute a high Q mode at $kR = 3.2$ in the same limaçon cavity as Fig. 1. The intensity maxima for the CW and CCW waves are spatially separated. The black dashed line describes the classical ray orbit with three bounces from the cavity boundary (labeled 1-3). The solid lines depict the path for the CW beam in (a) and CCW beam in (b), reconstructed from the incident and emergent Husimi distributions. The split in the CW and CCW orbits is due to GHS and FF. (c) The CW wave intensity is enhanced outside the cavity to show that the emission is predominantly from bounce 1 in the $\theta = 0°$ direction. (d) CCW wave intensity for a high Q mode at $kR = 5.2$, which is localized on a diamond orbit with four bounces from the cavity boundary. The classical ray orbit coincides with the paths for the CCW beam (solid line), extracted from the incident and emergent Husimi distributions. A similar result is obtained for the CW wave, whose pattern is the mirror image of the CCW wave with respect to the horizontal axis. (e) Local chirality $W(\theta)$ for the high Q modes at $kR = 3.2$ (solid line) and $kR = 5.2$ (dashed line). The former displays local chirality while the latter does not. (f) The far-field emission intensity I as a function of the polar angle θ for the two modes at $kR = 3.2$ (solid line) and $kR = 5.2$ (dashed line). The former has unidirectional emission and the latter is non-directional.

either CW or CCW inside the cavity to a waveguide placed tangentially to the cavity boundary, providing dominant output in *one* waveguide direction. To optimize the position of the waveguide, we numerically studied the dependence of evanescent coupling on the waveguide location along the boundary. Figure 4 presents the results for a cavity whose shape is close to the limaçon and described in the polar coordinates as $r(\theta) = R[1+\epsilon\cos(\theta)][1-\epsilon_1\cos(2\theta)]+d$, where $R = 890$ nm, $\epsilon = 0.28$, $\epsilon_1 = 0.06$, and $d = 60$ nm. A straight waveguide with the same refractive index as the disk is separated from the disk boundary by 100 nm and the

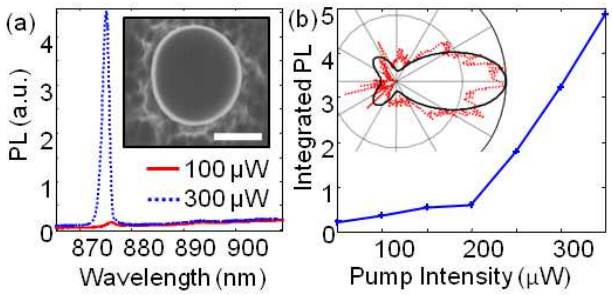

FIG. 3. (color online). (a) Measured photoluminescence (PL) spectra from a limaçon cavity of $R = 460$ nm and $\epsilon = 0.41$ at two incident pump powers: 100 μW (red solid line) and 300 μW (blue dotted line). The inset is the top-view SEM image of the disk, and the scale bar is 500 nm. (b) Intensity of the emission peak at $\lambda = 875$ nm in (a) as a function of the incident pump power. The threshold behavior indicates the onset of lasing action. The inset is a polar plot of the measured far-field pattern of laser emission (red dotted line) which agrees well with the calculated output of the high Q mode at the same wavelength (black solid line).

location of the coupling point is specified by the polar angle θ. At each θ, we calculated the steady-state intensity of emission coupled to the waveguide in the CW direction, J_{CW}, and the CCW direction, J_{CCW}. We present the behavior of a mode with $kR = 4.1$ although similar behavior was observed for other modes. We found that directional coupling is possible provided the waveguide is positioned in a region with local chirality. For example, if the waveguide is positioned at $\theta = 45°$, where the local amplitude of the CCW beam is highest, emission is mostly coupled in the CCW direction [Fig. 4(a)]. Figure 4(b) plots the directionality of the coupled emission $V \equiv (J_{CCW} - J_{CW})/(J_{CCW} + J_{CW})$ as a function of the coupling position θ. As the coupling point moves along the cavity boundary, the sign of $V(\theta)$ changes, indicating a switch in the direction of the evanescent waveguide coupling. To confirm that the directional coupling results from local chirality, we calculate the local chirality $W(\theta)$ for the same mode in the cavity without a waveguide. As shown in Fig. 4(d), the variation of $W(\theta)$ with θ mirrors that of $V(\theta)$ in Fig. 4(b), verifying the relation between the local chirality and the evanescent coupling to the waveguide.

To demonstrate this process experimentally, we fabricated waveguide-coupled cavities using the same procedure described above. A 250 nm wide GaAs waveguide was separated from the disk edge by a 100 nm air gap, and the coupling positions were chosen to yield

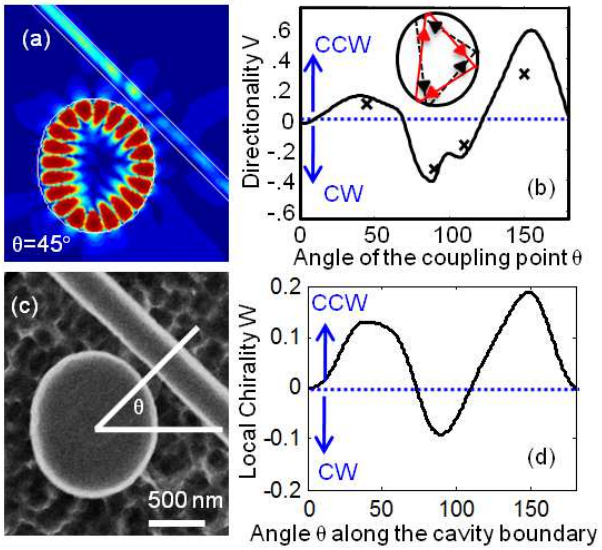

FIG. 4. (color online). (a) Calculated intensity distribution in a waveguide coupled deformed microdisk, showing directional coupling to a waveguide positioned at polar angle $\theta = 45°$. (b) Directionality of waveguide coupling V as a function of the coupling position θ on the cavity boundary. $V > 0$ ($V < 0$) corresponds to stronger coupling in the CCW (CW) direction. The crosses represent the experimental data points which agree well with the numerical simulation (solid line). The inset shows the orbits for the CW and CCW beams for this mode. (c) Top-view SEM image of a GaAs disk coupled to a waveguide. The disk is supported on an $Al_{0.7}Ga_{0.3}As$ pedestal at the center, and the GaAs waveguide is free standing in air and supported by two $Al_{0.7}Ga_{0.3}As$ pedestals at the ends. The background shows the residual $Al_{0.7}Ga_{0.3}As$ on the GaAs substrate after selective etching of the $Al_{0.7}Ga_{0.3}As$. (d) Local chirality $W(\theta)$ for the same mode in the absence of waveguide coupling. Locally, the CW and CCW intensities are not equal, leading to directional output to the waveguide shown in (b). Only half of the cavity boundary is plotted in (b,d), the other half can be obtained by mirror symmetry.

directional coupling. Figure 4(c) shows a SEM image of one of the GaAs disks with a coupled waveguide at $\theta = 45°$. The cavity shape is identical to the simulated one in Fig. 4(a). The waveguide was suspended in air by two $Al_{0.7}Ga_{0.3}As$ pedestals (not shown). We achieved lasing with optical pumping and observed similar threshold behavior to what was presented above for the cavity without a waveguide. To monitor the directional coupling, we imaged the emission scattered by the two pedestals at the ends of the waveguide. A narrowband interference filter was placed in front of the camera to select a single lasing mode for imaging.

By measuring the intensities of scattered light from the two pedestals, we obtained V. The experimental data points for the same cavity mode coupled to the waveguide at four different locations are plotted in Fig. 4(b) and show good agreement with the numerical simulations. We characterized the waveguide coupling of several cavities of different sizes, and obtained similar directional coupling [34].

Finally, we emphasize that the geometric shape of the cavities studied above maintains the chiral symmetry, $r(-\theta) = r(\theta)$, thus the cavity resonances do not possess *global* chirality, i.e., $\int_0^{2\pi} I_{CW}(\theta)d\theta = \int_0^{2\pi} I_{CCW}(\theta)d\theta$, which we confirmed numerically. Hence, chirality is introduced only locally [Fig. 4(d)] and it allows us to selectively couple either the CW or CCW wave by adjusting the waveguide location on the cavity boundary.

In conclusion, we have achieved lasing in deformed cavities of kR as small as 3. At such small values of kR, the paths of the CW and CCW propagating beams that constitute a resonance are spatially split by the Goos-Hänchen shift and the Fresnel filtering effect. Local chirality is introduced via the unbalanced amplitudes of local CW and CCW waves along the cavity boundary. This local chirality not only leads to unidirectional emission in free space, but also allows for directional evanescent coupling to a waveguide. These results illustrate that local chirality can be created by wave optics effects in ultrasmall resonators and utilized to control the output directionality and enhance the emission collection efficiency.

We thank Profs. A. Douglas Stone and Eugene Bogomolny for stimulating discussions. This work is supported partly by NSF under the Grant Nos. ECCS-1068642, ECCS-1128542, and by the DFG research group 760. Facilities use was supported by YINQE and NSF MRSEC DMR 1119826.

[1] S. McCall, A. Levi, R. Slusher, S. Pearton, and R. Logan, Appl. Phys. Lett. **60**, 289 (1992).

[2] T. J. Kippenberg, J. Kalkman, A. Polman, and K. J. Vahala, Phys. Rev. A **74**, 051802 (2006).

[3] K. Srinivasan and O. Painter, Nature **7171**, 862 (2007).

[4] S. J. Choi, K. Djordjev, S. J. Choi, and P. Dapkus, IEEE Photon. Tech. Lett. **15**, 1330 (2003).

[5] G. Chern, H. Tureci, A. Stone, R. Chang, M. Kneissl, and N. Johnson, Appl. Phys. Lett. **83**, 1710 (2003).

[6] X. Luo and A. W. Poon, Opt. Express **15**, 17313 (2007).

[7] J. Wiersig, Opt. Express **16**, 5874 (2008).

[8] X. Luo, H. Chen, and A. Poon, Opt. Express **16**, 5876 (2008).

[9] J. Nöckel, A. Stone, and R. Chang, Opt. Letters **19**, 1693 (1994).

[10] J. Nöckel and A. Stone, Nature **385**, 45 (1997).

[11] C. Gmachl, F. Capasso, E. Narimanov, J. U. Nöckel, A. D. Stone, J. Faist, D. L. Sivco, and A. Y. Cho, Science **280**, 1556 (1998).

[12] T. Harayama, T. Fukushima, S. Sunada, and K. S. Ikeda, Phys. Rev. Lett. **91**, 073903 (2003).

[13] M. Lebental, J. Lauret, R. Hierle, and J. Zyss, Appl. Phys. Lett. **88**, 1 (2006).

[14] J.-W. Ryu, S.-Y. Lee, C.-M. Kim, and Y.-J. Park, Phys. Rev. E **73**, 036207 (2006).

[15] S.-B. Lee, J. Yang, S. Moon, J.-H. Lee, K. An, J.-B. Shim, H.-W. Lee, and S. W. Kim, Phys. Rev. A **75**, 011802 (2007).

[16] J. Gao, P. Heider, C. J. Chen, X. Yang, C. A. Husko, and C. W. Wong, Appl. Phys. Lett. **91**, 181101 (2007).

[17] J. Wiersig and M. Hentschel, Phys. Rev. Lett. **100**, 033901 (2008).

[18] Q. Song, W. Fang, B. Liu, S.-T. Ho, G. S. Solomon, and H. Cao, Phys. Rev. A **80**, 041807 (2009).

[19] C. Yan, Q. J. Wang, L. Diehl, M. Hentschel, J. Wiersig, N. Yu, C. Pflügl, F. Capasso, M. Belkin, T. Edamura, M. Yamanishi, and H. Kan, Appl. Phys. Lett. **94**, 251101 (2009).

[20] S. Shinohara, M. Hentschel, J. Wiersig, T. Sasaki, and T. Harayama, Phys. Rev. A **80**, 031801 (2009).

[21] C.-H. Yi, M.-W. Kim, and C.-M. Kim, Appl. Phys. Lett. **95**, 141107 (2009).

[22] H. Schwefel, N. Rex, H. Tureci, R. Chang, A. Stone, T. Ben-Messaoud, and J. Zyss, J. Opt. Soc. Am. B **21**, 923 (2004).

[23] Q. H. Song, L. Ge, A. D. Stone, H. Cao, J. Wiersig, J.-B. Shim, J. Unterhinninghofen, W. Fang, and G. S. Solomon, Phys. Rev. Lett. **105**, 103902 (2010).

[24] J.-B. Shim, J. Wiersig, and H. Cao, Phys. Rev. E **84**, 035202 (2011).

[25] N. B. Rex, H. E. Tureci, H. G. L. Schwefel, R. K. Chang, and A. D. Stone, Phys. Rev. Lett. **88**, 094102 (2002).

[26] H. E. Tureci and A. D. Stone, Optics Letters **27**, 7 (2002).

[27] H. Schomerus and M. Hentschel, Phys. Rev. Lett. **96**, 243903 (2006).

[28] J. Unterhinninghofen, J. Wiersig, and M. Hentschel, Phys. Rev. E **78**, 016201 (2008).

[29] E. Altmann, G. Del Magno, and M. Hentschel, Europhys. Lett. **84**, 10008 (2008).

[30] J. Unterhinninghofen and J. Wiersig, Phys. Rev. E **82**, 026202 (2010).

[31] E. Narimanov, H. G., J. P., and S. A. D., Phys. Rev. Lett. **83**, 4991 (2012).

[32] See Supplementary Materials.

[33] M. Hentschel, H. Schomerus, and R. Schubert, Europhys. Lett. **62**, 636 (2003).

[34] B. Redding, L. Ge, G. Solomon, and H. Cao, Appl. Phys. Lett. **100**, 061125 (2012).